Soft Matter

PAPER

View Article Online
View Journal | View Issue

Cite this: *Soft Matter*, 2016, 12, 6400

Changes in the bending modulus of AOT based microemulsions induced by the incorporation of polymers in the water core

Björn Kuttich,* Ann-Kathrin Grefe and Bernd Stühn

Received 31st May 2016,
Accepted 5th July 2016

DOI: 10.1039/c6sm01253a

www.rsc.org/softmatter

The bending modulus κ is known to be a crucial parameter for the stability of the droplet phase in microemulsion systems. For AOT based water in oil microemulsions the bending modulus of the surfactant has values close to k_BT but can be influenced by the presence of polymers. In this work we focus on the water soluble polymer polyethylene glycol and how it influences the bending modulus. An increase by a factor of three is found. For the correct evaluation of the bending modulus *via* percolation temperatures and droplet radii, thus by dielectric spectroscopy and small angle X-ray scattering, the determination of the radii right at the percolation temperature is crucial as we will show, although it is often neglected. In order to precisely determine the droplet radii we will present a global fitting model which provides reliable results with a minimum number of free fitting parameters.

1 Introduction

A microemulsion is a thermodynamically stable mixture of a hydrophilic and a hydrophobic component stabilised by the presence of a surfactant.[1] The evolving micro-structure may be considered to consist of domains with dimensions on the nanometre length scale. These liquids are therefore optically transparent and macroscopically isotropic. Details of the micro-structure depend on the type of surfactant used and the mixing ratio as well as on temperature. The domain form varies with composition from lamellar and bicontinuous to spherical. In particular the latter has attracted large interest in fundamental and applied research. The selective solubility of guest molecules confines them within the nano-droplets of the microemulsion. Depending on the surfactant the system may favour water droplets embedded in an oil matrix (w/o) or the opposite arrangement (o/w). The size of the droplet and therefore the strength of confinement can be tuned mainly by the mixing ratio but is often also weakly dependent on temperature.[2–7]

The surfactant layer separating hydrophilic and hydrophobic domains is soft in the sense that thermal energy is sufficient to cause fluctuations. Its rigidity is described by the bending modulus.[8,9] Moreover droplets are Brownian particles diffusing in the continuous phase of the microemulsions. They will collide and exchange materials. The confinement of guest molecules is therefore called a soft confinement.

Experimental Condensed Matter Physics, TU Darmstadt, Germany.
E-mail: b.kuttich@fkp.physik.tu-darmstadt.de; Tel: +49 6151 16 2584

In recent years microemulsions in the droplet phase have been used as such soft confining geometry for many different molecules like glass forming liquids, polymers or proteins.[4,10–12] A key question in these studies has been the stability of the microemulsion system itself under the influence of the added molecules. It is indeed found that additives have a significant impact on the phase boundaries of the droplet phase.[13,14] The concentration of added molecules in these studies is low and amounts to a few molecules per droplet.

Two well suited complementary measuring methods for the investigation of phase stability in microemulsions are small angle scattering and dielectric spectroscopy. The first one provides detailed information on the structural properties of the system and allows a temperature resolved determination of droplet radii and their distribution.[3–5] Furthermore interdroplet interactions leading for example to the aggregation of droplets can be investigated.[3,5] Dielectric spectroscopy gives access to the conductivity of the system. Charge transport is very sensitive to phase changes in a microemulsion especially for w/o systems. It gives rise to the so called percolation transition, an increase of conductivity over several orders of magnitude due to quite a small change in temperature.[13–17]

Connecting the information from small angle scattering and dielectric spectroscopy allows us to access a fundamental quantity for the stability of the droplet phase, the bending modulus of the surfactant shell.[17–19] In microemulsion systems the bending modulus is usually of the same size as k_BT which makes the micro-structure appear rather floppy. It fluctuates on a nanosecond time scale.[17,20,21] Being so close to the thermal energy of the system already small changes of the bending modulus

due to the insertion of guest molecules into the core of the droplets can strongly change the phase properties of the microemulsion.

In the present study we focus on microemulsions based on the anionic surfactant dioctyl sodium sulfosuccinate (AOT) which favours a w/o droplet phase over a broad range of temperatures and mixing ratios. The continuous oil phase is octane and the water cores of the droplets contain the water soluble polymer polyethylene glycol. Droplet size and polymer concentration are varied systematically in order to provide different confining situations and stability of the droplets *i.e.* the bending modulus is investigated. In order to reliably determine the bending modulus from small angle X-ray scattering and dielectric spectroscopy, especially in the case of polymer loaded droplets, both experimental techniques have to be performed in a range of well-defined temperature. This fact which is often not considered for the scattering experiments but as we will show it is absolutely mandatory.

2 Experimental details

2.1 Sample preparation

Preparation of the different microemulsions was done by weighing appropriate amounts of surfactant, water, oil and polymer on a microbalance and mixing these components using a vortex shaker. After preparation the samples are stored in sealed borosilicate glasses at room temperature. They are stable over several years. Water was taken from a Millipore Direct-Q3 ultrapure water system. The surfactant AOT was purchased from Sigma Aldrich. The polymer was obtained from Alfa Aesar with a mean molecular weight of M_n = 4000 g mol^{-1} (PEG4000). Both the polymer and the surfactant were dried for 24 hours at 45 °C in a vacuum oven before sample preparation. The composition of the microemulsion is defined using the parameters w and ϕ. w denotes the molar ratio of water to surfactant molecules and ϕ denotes the volume fraction of water plus surfactant. For droplet phase microemulsions this parametrisation is very convenient since w is proportional to the droplet radius and ϕ directly gives the droplet volume fraction.[22] To quantify the amount of polymers in the samples the parameter Z is introduced calculated by the average number of polymer chains per droplet. For our experiments we chose to keep the droplet volume fraction constant at ϕ = 0.1 and vary w between 20 and 40 yielding water core radii from 28 Å to 56 Å approximately.[22] The number of polymers per droplet is varied between Z = 0 and Z = 3. This corresponds to polymer in water concentrations up to 18% which is close to the estimated overlap concentration of PEG4000 of 24%.[23]

To perform the measurements samples were filled in borosilicate capillaries with a diameter of 1.5 mm for the small angle X-ray scattering experiments or a sample holder similar to that described in ref. 24 for dielectric spectroscopy. Since some of the highly polymer loaded systems are no longer in the one phase microemulsion region at room temperature special care has to be taken for their measurement. To ensure that the measurement, small angle X-ray scattering as well as dielectric spectroscopy, always begins in the one phase droplet region of the system all parts starting from the storage glass, *via* the syringes used, the sample cell and the instrument were heated up to a temperature at which the sample was in the one phase region. Then the sample was filled as quickly as possible in the sample cell and inserted in the instrument without dropping below the phase separation temperature and the measurement started at this chosen temperature.

2.2 Small angle X-ray scattering

2.2.1 Experimental set-up. Small angle X-ray scattering was performed using a laboratory Kratky compact camera by Anton-Paar. We use the K_α-line of a copper X-ray tube with a wavelength of λ = 1.54 Å monochromated by a nickel filter and collimated by a slit collimation system. Measured data were desmeared by an algorithm proposed by G. Strobl.[25] Desmeared data are presented as intensity *versus* modulus of the scattering vector $q = \frac{4\pi}{\lambda}\sin\phi$, with 2ϕ being the scattering angle. The sample temperature was monitored using a PT100 platinum resistance thermometer and controlled *via* a Eurotherm controller with an accuracy of 0.2 K. Prior to each measurement the sample was equilibrated at the given temperature for 300 s.

2.2.2 Data evaluation. The measured scattered intensity of the isotropic polydisperse droplets can be written as

$$I(q) \propto \langle F(q)\rangle^2 S(q) + \langle F(q)^2\rangle - \langle F(q)\rangle^2 \quad (1)$$

with $F(q)$ denoting the form factor of the droplets. It is the Fourier transform of the scattering length density of the particle and in this way it describes the shape of the scattering particle. $\langle\cdots\rangle$ denotes an ensemble average. $S(q)$ is the structure factor taking interparticle scattering into account.[26] Scattering is caused by the difference in electron density of the components. For our system the dominant contribution is caused by the difference between the hydrophilic head groups of the surfactant and the water core causing a pronounced shell contrast.[5] The form factor was calculated for spherical core–shell particles as given in ref. 2:

$$F(q) = r_c^3 \Delta\rho_{cs} \frac{\sin(qr_c) - qr_c\cos(qr_c)}{(qr_c)^3} + R^3 \Delta\rho_{sm} \frac{\sin(qR) - qR\cos(qR)}{(qR^3)} \quad (2)$$

Here r_c is the core radius, the polar radius is denoted by $R = r_c + \delta$ with the shell thickness δ defined by the surfactant head group. $\Delta\rho_{cs}$ is the difference in scattering length density between the core and the shell and $\Delta\rho_{sm}$ between the shell and the matrix. The surfactant tail has almost the same electron density as the surrounding oil matrix and can therefore not be determined by small angle X-ray scattering. The polydispersity of the droplet radii was taken into account by averaging intensity with a Schulz–Zimm distribution of the core radius.[3]

For the structure factor we chose a combination of the phenomenological Ornstein–Zernike structure factor[3] and a

hard-sphere structure factor[27] as it is explained by Domschke *et al.*[5] The Ornstein–Zernike structure factor is expressed as

$$S(q) = \frac{\chi}{1 + \xi^2 q^2}, \tag{3}$$

with a susceptibility $\chi \propto k_B T \kappa_O$, introducing the isothermal osmotic compressibility κ_O, and a correlation length ξ. The hard-sphere structure factor is given by

$$S(q) = \frac{1}{1 + 24\eta \frac{G(q, R_{HS})}{2qR_{HS}}} \tag{4}$$

with a periodical function $G(q,R_{HS})$, the volume fraction of hard spheres η and their radius R_{HS}.

The overall number of fitting parameters of the described model is five for the form factor (core radius r_c, radius polydispersity σ, shell thickness δ, scattering contrast core–shell $\Delta\rho_{cs}$ and scattering contrast shell–matrix $\Delta\rho_{sm}$), four for the two structure factors (susceptibility χ, correlation length ξ, hard-sphere volume fraction η and radius R_{HS}) and an additional pre-factor resulting in ten fitting parameters in total. This number can be significantly reduced by fixing several parameters to their known values from literature. For the form factor these are the scattering length densities for the core $\rho_c = 9.4 \times 10^{-6}$ Å^2, the polar head group of the shell $\rho_s = 23.9 \times 10^{-6}$ Å^2 and the surrounding matrix $\rho_m = 6.88 \times 10^{-6}$ Å^2.[28,29] Furthermore the thickness of the polar AOT head group is independent of the sample composition and temperature and given by $\delta = 2.1$ Å.[5] For the hard-sphere structure factor the radius can be estimated by $R_{HS} = r_c + \delta + L_{AOT}$ with $L_{AOT} = 10.5$ Å being the length of the alkane tails of the AOT molecule.[2,5,30] So if every single scattering curve is fitted individually the final number of free fitting parameters is six per sample and temperature.

For a scattering curve with pronounced minimum due to the form factor and precisely measured low q-range to cover the structure factor six parameters are expected to be an adequate number of free fitting parameters. Thus the results of the fitting procedure promise to be reliable. Nevertheless the different contributions discussed for the scattering profile overlap in the observed range of scattering vectors $\boldsymbol{q}$. This may lead to correlations between different fitting parameters which make their reliable determination a difficult task. In order to deal with these correlations we make use of known relations between the different structure factor parameters and system parameters like temperature and droplet size. We use these relations to fit multiple data sets taken in a range of temperatures and for different droplet size in one step. This method of global fitting will allow us to determine even the otherwise correlated structure factor parameters precisely and reliably.

By increasing the temperature it is possible to leave the stable one phase droplet region and to obtain a demixed two phase system. This demixing takes place at a temperature T_c which is called the phase separation temperature. At this temperature the system undergoes a second order phase transition which is directly related to critical fluctuations within the sample.[3,5,31] Due to this phase transition several quantities obey a power law behaviour while approaching T_c. This applies to the susceptibility χ and the correlation length ξ included in the Ornstein–Zernike structure factor part.[32] As has been shown by several authors the temperature dependence on the susceptibility and the correlation length can be written as

$$\chi(T) = \chi_0 \cdot \theta^{-\gamma}$$
$$\xi(T) = \xi_0 \cdot \theta^{-\nu} \tag{5}$$

where $\theta = (T_c - T)/T_c$ is the normalised distance to the phase transition temperature and γ and ν are critical exponents for which the relation $\gamma = 2\nu$ should hold.[3,5,31,32] Furthermore Domschke *et al.* have shown that besides the critical exponents the factor χ_0 is independent of droplet size and only depends on droplet concentration ϕ while the pre-factor $\xi_0 = \xi_w \cdot w$ shows a linear dependency on the molar water to surfactant ratio w.[5] Due to these properties of the Ornstein–Zernike structure factor the number of free fitting parameters can be further reduced significantly, if a series of microemulsions with different w and at temperatures up to the phase transition temperature T_c is measured. Taking the $Z = 0$ w-series we investigated as an example, the total number of scattering curves recorded is 42. This results in $42 \times 2 = 84$ fitting parameters for the Ornstein–Zernike structure factor part only, if the scattering curves are fitted independently. Using the relations described above the number of fitting parameters can be reduced to four, namely the two critical exponents γ and ν and the two pre-factors χ_0 and ξ_w respectively.

Finally the hard-sphere volume fraction η can be addressed. Domschke *et al.* concluded from their investigations that at higher temperatures the Ornstein–Zernike structure factor part becomes stronger due to droplet clustering, and the number of free droplets interacting like hard spheres is reduced.[5] They found that this decrease is linear with increasing temperature which allows further reduction of the free fitting parameters since the hard-sphere volume fraction can be written as:

$$\eta(T) = \eta(25\,^\circ\mathrm{C}) + \frac{\eta(T_c) - \eta(25\,^\circ\mathrm{C})}{T_c - 25\,^\circ\mathrm{C}} \cdot T \tag{6}$$

Thus for every temperature series with constant ϕ, w and Z only two free fitting parameters for the hard-sphere structure factor remain, namely $\eta(25\ ^\circ\mathrm{C})$ and $\eta(T_c)$ the hard-sphere volume fraction at 25 °C and at the phase separation temperature T_c respectively.

In conclusion the total number of free fitting parameters for the 42 scattering curves mentioned above is now not $42 \times 6 = 252$ as for an individual fitting procedure but down to 132 due to the global fitting which results in an average of 3.1 parameters per scattering curve. The merit of this fitting technique is that possible correlations between the different structure factor parameters are already incorporated in a physical reasonable way in accordance with the literature.[3,5,31]

2.3 Dielectric spectroscopy

For the dielectric spectroscopy a Novocontrol Alpha-N High Resolution Dielectric Analyzer was used with frequencies ranging

from 10^1 Hz to 10^7 Hz. Dielectric spectroscopy measures the frequency dependent complex impedance $Z^*(f)$ from which the dielectric function $\varepsilon^*(f)$ can be calculated by $\varepsilon^*(f) = (2\pi i f Z^*(f) C_0)^{-1}$, with C_0 denoting the capacitance of the empty capacitor. In this publication we analyse the real part $\sigma'(f)$ of the complex conductivity $\sigma^*(f)$, which is related to the dielectric function *via* $\sigma^*(f) = 2\pi i f \varepsilon_0 \varepsilon^*(f)$. The relative uncertainties of the measured complex conductivities during one measurement are below one percent. However the errors of the absolute values of σ' and σ'' are mainly determined by the uncertainties of capacitor geometry and are estimated to be about 2%. The sample temperature was controlled using a Novocontrol Quatro Cryosystem with a temperature stability better than ± 0.1 K and an absolute accuracy of ± 0.5 K. All temperature dependent measurements were performed in heating runs, with 300 s stabilisation time at each measured temperature.

The dc conductivity of a w/o microemulsion is in general very low, around $\sigma_{dc} = 10^{-8}$ S cm^{-1}, due to the resistance of the oil continuous matrix.[6,13] It is larger than that of the pure oil because droplets can carry net charges and therefore act as huge ions diffusing through the oil. This mechanism is described by the charge fluctuation model.[33,34] If either droplet concentration or temperature in such a system is increased, conductivity can rise dramatically up to four orders of magnitude because of a phenomenon called dynamic percolation. It is caused by an attractive force between the droplets.[6,35–37] As a consequence of this droplets start to form aggregates and at the percolation threshold an extended droplet cluster from one electrode to the other is formed. Charge transport therefore changes its mechanism from charge fluctuation and Brownian transport to conductivity along the cluster. If droplet concentration or temperature is increased even further the system eventually passes the phase boundary and decomposes into a two phase system which leads to a sharp drop in the measured conductivity. The precise temperature or droplet concentration at which the percolation and the phase transition occur depends on the droplet size as well as on the amount of polymers inserted into the water core.[13]

We use temperature as the controlled parameter to study percolation and phase separation. To obtain the percolation T_p and the phase separation T_c temperature the temperature dependence on the complex dielectric conductivity was studied at a frequency of 10^4 Hz. This frequency was chosen because there are no disturbing effects from electrode polarisation or dielectric relaxations present.[13] The percolation temperature was then determined as the inflexion point of the logarithmic conductivity plotted *versus* temperature, while the phase separation temperature was taken from the last point before the final drop in conductivity.[13]

2.4 Determination of the bending modulus

The bending modulus κ of the surfactant layer controls the extent of form fluctuations and the percolation temperature. Therefore from a combination of structural information as the droplet sizes and thermodynamic properties like the percolation temperature it is possible to determine the bending modulus κ of the surfactant shell.[17,18] In order to distinguish large and small length scales of fluctuations in a microemulsion De Gennes and Taupin introduced the so called persistence length ξ_K of the surfactant shell.[9] For distances smaller than ξ_K the surfactant layer looks smooth and flat while for larger distances it is crumpled.

Furthermore, they concluded that the persistence length should obey the following Arrhenius type equation[9]

$$\xi_K = a \exp\left[\frac{2\pi\kappa}{k_B T}\right], \tag{7}$$

where $k_B T$ is the thermal energy and a is a quantity related to the size of a surfactant molecule. This conclusion was later refined by Gompper and Kroll considering undulation modes along the surfactant interface, leading to a renormalisation of the bending modulus.[19,38] In order to determine the persistence length Meier made the assumption that at the percolation temperature T_p the persistence length should match the droplet radius r_c and thus eqn (7) can be rewritten as ref. 18:

$$r_c = a \exp\left[\frac{2\pi\kappa}{k_B T_p}\right] \tag{8}$$

This relation allows us to calculate the bending modulus of the surfactant shell by measuring the percolation temperature of droplet phase microemulsions with different radii.

2.5 Temperature calibration

In the following we will combine results from dielectric spectroscopy and small angle X-ray scattering. In particular the precise phase separation temperature T_c is needed to be used in the global fitting procedure of scattering data. The percolation temperature T_p has to be known for the calculation of the bending modulus. In both cases the equivalence between temperatures measured in the dielectric spectrometer and the small angle X-ray scattering device is absolutely crucial for correct results. In order to check this equivalence a calibration substance is needed whose structural and dielectric properties change depending on temperature in a way that it can be resolved by both experimental techniques. This will allow us to determine the possible difference in the actual sample temperatures in both experimental setups.

Excellent candidates for this purpose are liquid crystals. In a liquid crystal the phase transition between the nematic and the isotropic phase can be measured by a reduction in the dielectric permittivity as well as by the disappearance of the nematic order peak. For the relevant temperature range between 25 °C and 75 °C we found two liquid crystals with a nematic to isotropic transition, 5CB and E7. The liquid crystal 5CB has a phase transition temperature around 36 °C while this temperature for E7 is 60 °C.[39,40]

In Fig. 1 the phase transition temperature as measured by broadband dielectric spectroscopy (BDS) is plotted against the corresponding temperature observed in small angle X-ray scattering (SAXS). Physically the reduction of the permittivity and the vanishing of the structure peak should occur at the same temperature thus the two data points should be located

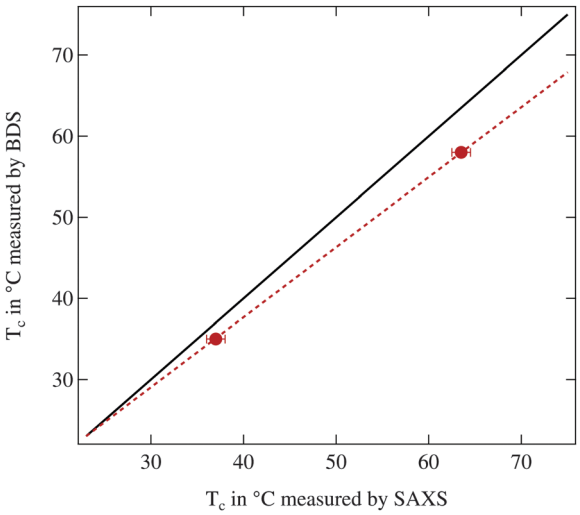

Fig. 1 Phase transition temperature T_c of the liquid crystals 5CB and E7 as measured by broadband dielectric spectroscopy (BDS) and small angle X-ray scattering (SAXS). The solid line is the bisection as guides for the eye while the dashed line is a linear fit to the data points (see text for details).

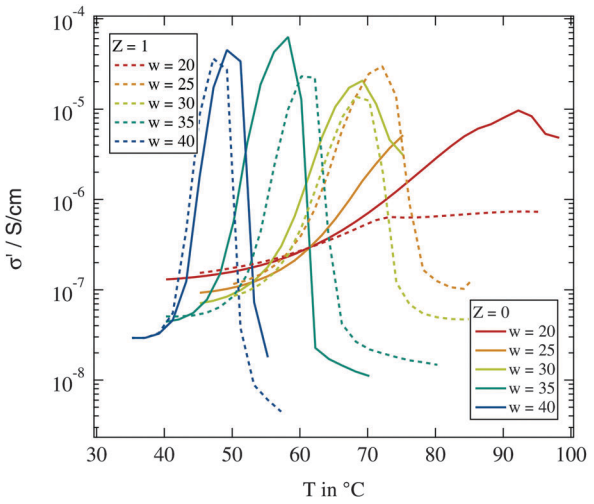

Fig. 2 Real part of the dielectric conductivity at $f = 10^4$ Hz for different droplet sizes and polymer contents.

on the bisecting line. As can be clearly seen this is not the case and the phase transition temperatures determined by SAXS are significantly increased in comparison to the ones from BDS. Therefore a calibration line is calculated assuming that in thermal equilibrium at room temperature both setups show the same temperature and at higher temperatures a linear offset is present, quantified by the two measured reference values. In the following we use this calibration line to match temperatures between both instruments.

Since the phase transition temperatures determined by BDS are closer to the literature values the temperatures from dielectric spectroscopy will be regarded as accurate temperatures while the temperatures from SAXS are recalculated using the calibration line. For the highest investigated temperature of 75 °C the deviation between both instruments is $\Delta T = 5.2$ K which demonstrates the necessity of the calibration procedure.

3 Results

3.1 Variation of transition temperatures with droplet size and polymer content

We start with the determination of percolation and phase separation temperature depending on the droplet size and the amount of polymers present in the system. We use the temperature variation of conductivity as described in Section 2.3. Fig. 2 shows the temperature dependent conductivity for different droplet sizes and for $Z = 0$ and $Z = 1$ polymer chains per droplet. For all investigated samples a rise of conductivity by orders of magnitude can be observed due to dynamic percolation. At even higher temperatures the conductivity collapses again because of the phase transition into two phase systems.

As described above the percolation temperature T_p can be determined from these conductivity data as the point of inflexion on the rising side while the phase separation temperature T_c is given by the temperature at which the conductivity starts to drop again. An increase of the molar water to surfactant ratio w and thus an increase in droplet size clearly lead to a reduction of both T_p and T_c. The influence of the polymer addition in contrast is not clear. An increase as well as a decrease of the percolation temperature with regard to the polymer free case can be observed. An overview of the observed percolation and phase separation temperatures for all investigated samples in this work is given in Fig. 3.

As can be seen both temperatures are overall decreasing with increasing water to surfactant ratio w as was observed before.[13] The influence of polymer content is less clear. While for large droplet sizes the changes due to the presence of the polymer are weak, it becomes more prominent for small droplets and larger polymer contents. For the latter case a decrease in both temperatures can be observed, and thus the temperature range of the droplet phase is reduced. For the largest droplets both temperatures seem to be elevated which has also been reported in the literature.[13,14,41]

Taking a closer look at the influence of droplet size on both temperatures another interesting feature of polymer addition becomes apparent. The polymer free system as well as the ones with $Z = 2$ and $Z = 3$ seems to show linearly decreasing percolation and phase separation temperatures with increasing w, at least as long as the $w = 25$ sample with $Z = 3$ is excluded. For the $Z = 1$ series, however, this appears to be different. At small droplet sizes an increase of w has almost no effect while for the large droplets the strongest decrease of all investigated series in both temperatures due to an increase in w can be seen. The number of data points available does not allow for a more detailed discussion of the variations. But it is useful to keep the particular behaviour for the $Z = 1$ series in mind while investigating the structural quantities.

In conclusion an analysis of percolation and phase separation temperature, quantities purely determined by dielectric spectroscopy, does not show a systematic influence of polymer

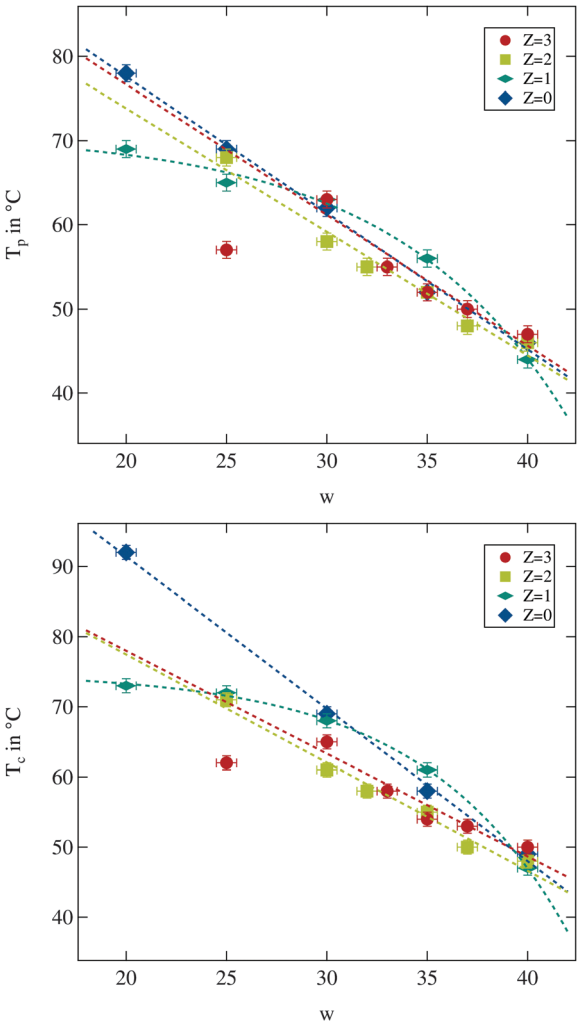

Fig. 3 Percolation temperature T_p and phase separation temperature T_c for different droplet sizes and polymer contents. Dashed lines are guides for the eye.

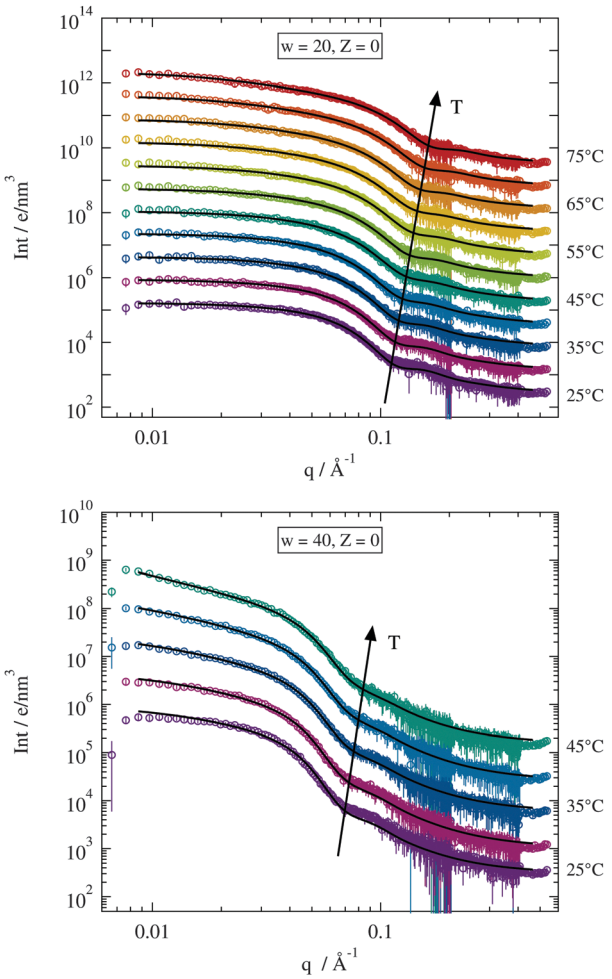

Fig. 4 Temperature dependent scattering curves for two chosen $Z = 0$ samples. Solid lines are fits of the model described in Section 2.2.2. Curves are vertically shifted for clarity.

addition on transition temperatures. In the following section we will discuss the results obtained by small angle X-ray scattering focussing on the impact of the added polymer on the microemulsion system.

3.2 Variation of droplet size and interaction

3.2.1 Quality of the SAXS fitting model. In Section 2.2.2 we described the complex fitting model used to evaluate the recorded data. Since a number of physical constraints are incorporated in this model it is important to thoroughly check the quality of the model in order to avoid forcing fitting parameters which are not supported by the data. In Fig. 4 two temperature series with $Z = 0$ are shown, for the $w = 20$ and the $w = 40$ samples. The depicted temperatures are given as an orientation and are therefore not corrected as discussed in Section 2.5. Due to a higher phase separation temperature for smaller droplets as seen in the results of the dielectric spectroscopy (Section 3.1) the low w sample (upper panel) was investigated up to higher temperatures.

For large scattering vectors ($q \gtrsim 0.08$ Å^{-1}) all scattering curves show a pronounced shoulder emerging from the spherical form factor. As expected this maximum shifts to lower q-values for larger w implying larger structures, while the increasing temperature has the opposite effect.[4,5,22,30] In the case of the $w = 40$ sample the maximum becomes more smeared for higher temperatures. This effect seems less pronounced in the $w = 20$ sample. Looking at the low q-range where the structure factor should dominate the scattering signal the $w = 20$ sample shows almost a horizontal trend typical for single particle scattering. The $w = 40$ sample on the other hand clearly exhibits an increasing power law behaviour in $I(q)$ with increasing temperature. This different behaviour for both droplet sizes is due to their different separation between percolation and phase separation temperature. As seen by dielectric spectroscopy the gap between T_p and T_c becomes systematically smaller for larger droplets. Since the scattering curves are only recorded up to the percolation temperature the distance to the phase separation is much larger for smaller droplets than for the bigger ones resulting in a less pronounced power law behaviour at low q-values.

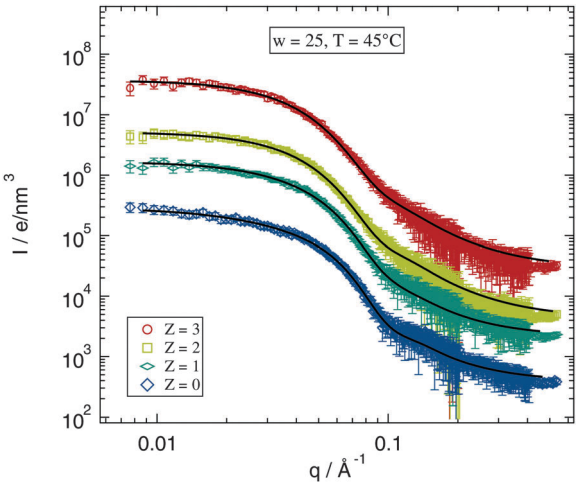

Fig. 5 Scattering curves for w = 25 and T = 45 °C with different number Z of polymer chains per droplet. Solid lines are fits of the model described in Section 2.2.2. Curves are shifted vertically for clarity.

The solid black lines in Fig. 4 represent collective fits by the model described in Section 2.2.2. The form factor part of this model is mostly dominated by the radius of the spherical water core r_c and its polydispersity σ. Both parameters are fitted individually to each scattering curve and this enables the model to describe the high q-range quite well. The structure factor parameters are adjusted globally to describe all the recorded data curves with $Z = 0$ at once. Here as well the model fits nicely the discussed features of the scattering curves at low q. Some minor deviations can be seen in the case of the $w = 40$ sample at $T = 25$ °C but even for this data set the model provides an acceptable description especially considering the low number of fitting parameters.

Since the fitting model describes in good agreement the $Z = 0$ samples the next question is, whether this works as well for the polymer loaded samples. The selected data shown in Fig. 5 allow for a direct inspection of the impact of the added polymer on the scattering profile. The figure shows scattering curves and fits for w = 25 and T = 45 °C for the investigated polymer concentrations. The differences between the scattering curves for various values of Z are obviously rather small. The form factor maximum around $q \approx 0.15$ Å^{-1} becomes slightly broader for higher polymer concentrations but this can still be described by the fitting model. The structure factor part does not seem to be influenced by polymer addition for the data shown. Thus also the low q-range is fitted well by the model.

The quality of the fitting model as discussed in this section is satisfactory for all recorded scattering curves. The main features of the form factor, the maximum at intermediate and high q-values, as well as the ones for the structure factors, especially the power law behaviour at temperatures close to the phase separation, are nicely described by the proposed model. Therefore we expect the resulting fitting parameters to be reliable and focus thus on their evaluation in the following sections.

3.2.2 Form factor parameters: droplet size and size distribution. For an analysis of the fitting parameters we will focus firstly on the two form factor parameters, the water core radius r_c and its polydispersity σ. It is known that the droplet radius scales linearly with the molar water to surfactant ratio w.[4,5,22,30] If the polydispersity of the water core radius is taken into account using Schultz–Zimm distribution the relation

$$(1 + 2\sigma^2) \cdot r_c = \frac{\langle r_c^3 \rangle}{\langle r_c^2 \rangle} = \frac{3v_w}{A_{AOT}} \cdot w = c \cdot w \qquad (9)$$

should hold. The factor c is deduced by geometrical considerations as the relation between the molar volume of a water molecule v_w and the effective surface area of the AOT head group A_{AOT}.[30] The latter one is only weakly dependent on the composition of the microemulsion for $w > 10$.[5,42–46] Its exact value can be measured using various scattering techniques as reported in the literature and results consistently in $c = 1.3$ Å $\pm$ 0.2 Å at room temperature.[4,5,22,30,42,43,46,47]

Furthermore the temperature dependency of c is discussed.[5,46,48–51] In the investigated temperature range the molar volume of water can be considered as a constant and thus temperature dependent changes in the droplet volume are due to the changing effective surface area of the AOT head group A_{AOT}. For ionic surfactants such as AOT a repulsive interaction between the head groups appears. The strength of this interaction depends on the presence of counter ions, dissolved in water, shielding the head groups against each other. By increasing the temperature the solubility of these ions is increased, the shielding reduced and thus the repulsion increases leading to a larger effective surface area of the droplets.[50] Due to the geometrical considerations of eqn (9) this leads to a reduced radius of the microemulsion droplets upon heating which is indeed observed in several studies.[5,46,48,51] Thus from now on we will refer to c as $c(T)$.

Since our fitting model described in Section 2.2.2 allows us to determine the water core radius of the droplets as well as its polydispersity we can now investigate $c(T)$ by plotting the scaled radius $(1 + 2\sigma^2)\cdot r_c$ against w as shown in Fig. 6 for various temperatures of all the samples from the $Z = 0$ and $Z = 3$ series. For both polymer concentrations the linear relation implied by eqn (9) is well established. A closer investigation nevertheless reveals some interesting differences. The fitted lines spread wider for the $Z = 3$ samples indicating an increased influence of temperature on those samples. For the two lowest investigated temperatures in contrast this does not seem to be the case since here the data points for the $Z = 3$ sample are almost identical. Furthermore the polymer loaded samples with $w \leq 30$ are clearly deviating from the linear relation predicted by eqn (9). This deviation to larger radii is most likely due to the presence of the polymer. Polymer size is characterized by its radius of gyration of $r_g \approx 25$ Å. Thus in the case of $Z = 3$ the polymer should be strongly confined by the droplets which may be expected to influence droplet radii in return.[52,53] The missing low temperature radii for the small polymer loaded droplets could not be measured because the polymer addition leads to an increase of the lower phase boundary thus the droplet phase becomes unstable below 40 °C for these samples.

A more detailed description of the impact of the polymer on the temperature variation of droplet size is obtained from the

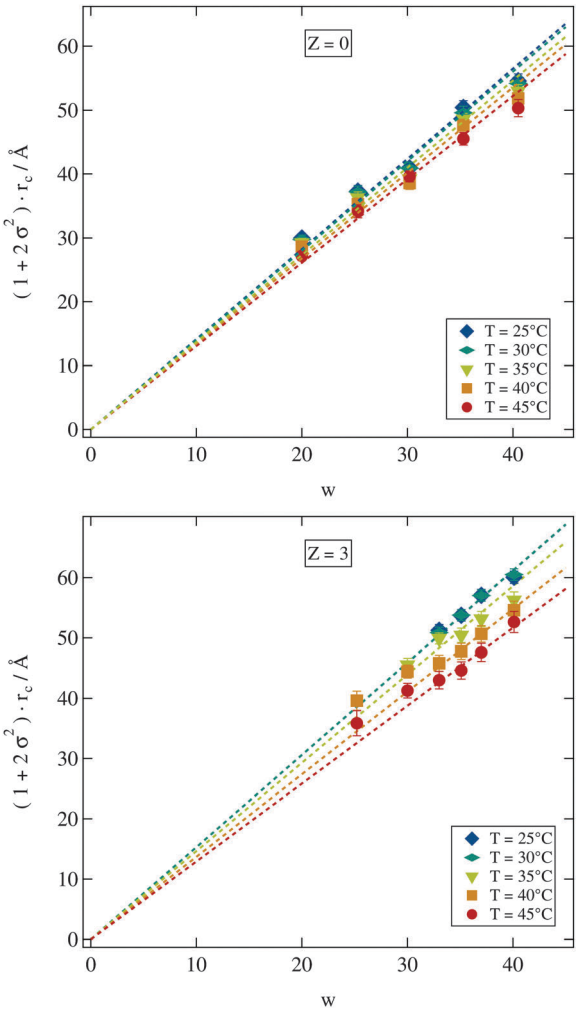

Fig. 6 Polydispersity σ scaled water core radius r_c shows a linear dependency on the molar ratio of water to surfactant w. Dashed lines are fits of eqn (9). Error bars are smaller than symbols if not visible.

quantity $c(T)$ in eqn (9). For fitting eqn (9) to the scaled radii the small w high Z samples with clearly deviating radii discussed above were excluded. Polymer free microemulsions should exhibit a linearly decreasing $c(T)$ with increasing temperature.[5] Indeed this same variation can be observed for the samples investigated in this work as shown in Fig. 7. A reduction of the proportionality constant with increasing temperature can also be seen for the polymer loaded samples but for $Z \geq 2$ the decrease is identical and not linear any more. For these high polymer concentrations a temperature increase around 25 °C has almost no effect which we have already seen in Fig. 6 for the $Z = 3$ series. At elevated temperatures $c(T)$ is strongly influenced by temperature and the proportionality constant drops rapidly with temperature. Besides the different temperature dependent behaviour for various Z values, there is a crossing point where all lines intersect. This point is at $T \approx 45$ °C and $c(T) \approx 1.3$. At this temperature an increase in the molar ratio of water to surfactant w leads to the same increase in the droplet radius independent of the presence of the polymer.

We now consider the direct impact of polymer addition at fixed droplet size and temperature. At $T = 40$ °C most of the

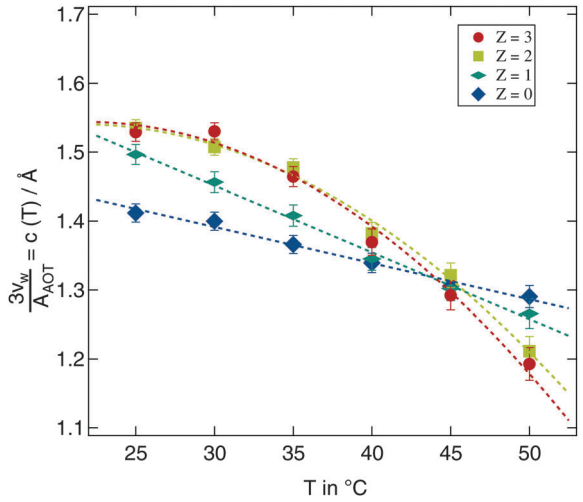

Fig. 7 Development of the proportionality constant $c(T)$ from eqn (9) for all investigated temperatures and polymer concentrations. Dashed lines are guides for the eye.

samples are in the non-percolated stable droplet phase for all polymer concentrations. We therefore choose this temperature in Fig. 8 to display the polydispersity scaled water core radii r_c for all stable samples at this temperature. Addition of the polymer does clearly lead to an increase in polydispersity and radius independent of the molar water to surfactant ratio w. With the exception of the filled symbols ($w = 35$) obviously the increase of the scaled radius per polymer chain can be described by straight lines with a w independent slope of 1.6 Å per polymer chain. Since this analysis is based on the polydispersity scaled radii which combines the influence of polymer addition on both quantities it is hard to relate the fitted slope to a structural property of the pure polymer.

Considering the slight change in the density of the polymer–water mixture in comparison to the pure water system the increase

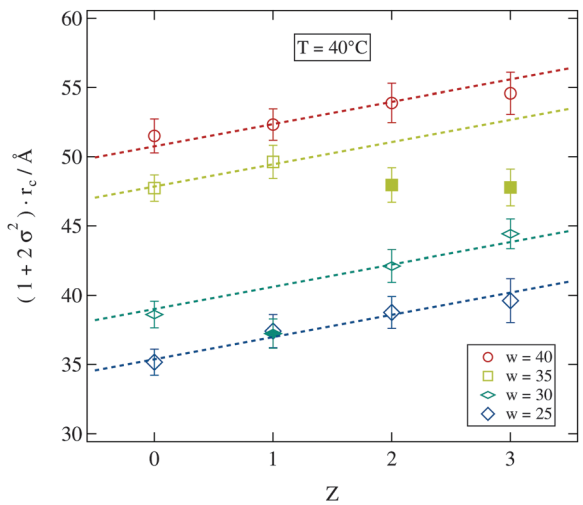

Fig. 8 Dependence of the scaled water core radius on the number of polymer chains per droplet Z. Dashed lines are guides for the eye with an identical slope.

in droplet volume due to the presence of the polymer can be estimated.[54] For one polymer chain in a $w = 30$ droplet the polymer in water mass concentration is $c = 0.02$ which leads to a relative increase in the droplet radius of about 1%. This is a much smaller effect than that observed here. Thus the polymer's influence on the microemulsion droplet has to be more complex than a simple volume change. In fact it is expected that PEG adsorbs at the water–AOT interface due to the presence of hydrophilic and hydrophobic groups of the polymer, which has a significant influence on the surfactant shell properties as we will see later.[13,18,55,56]

Droplet size is clearly influenced by the presence of the polymer. Polymer addition systematically affects both temperature and w dependence of the droplet radius and its polydispersity.

3.2.3 Variation of droplet interaction. In this section we study the variation of droplet interaction as seen in the structure factor of SAXS. To quantify the results of the SAXS measurement we focus on the Ornstein–Zernike part of the structure factor. More specifically we discuss the variation of the critical exponents γ and ν introduced in Section 2.2.2 with polymer addition. We will not analyse the hard-sphere volume fraction in detail since for a $\phi = 0.1$ microemulsion it is generally very low ($\eta \approx 0.05$)[5] and thus the hard-sphere structure factor part does not play an important role. This is in particular true around the percolation and phase separation temperatures where the structure factor is dominated by droplet clustering.[5,13]

The critical exponents acquired from the fitting model are shown in Fig. 9. The model assumes the critical exponents to be independent of the droplet radii, which is justified as discussed in Sections 2.2.2 and 3.2.1, and therefore only a possible variation of the critical exponents due to polymer addition may be expected. But even the addition of the polymer has no significant influence on both parameters. The dashed lines indicate two fitted constants to all shown data points with the condition $\gamma = 2\nu$ resulting in $\nu = 0.73$ and $\gamma = 1.46$ which is in good agreement with the literature.[3,5,31,57] Obviously the addition of the polymer does not change the occurrence of critical fluctuations approaching the phase separation temperature and thus the fundamental properties of the phase transition itself are unaffected.

Besides the critical exponents the pre-factors of the power laws included in the Ornstein–Zernike structure factor part (eqn (5)) can be obtained from the data. As opposed to the critical exponents these prefactors include specific properties of the system. Indeed they change strongly with the number of polymers added. For example the absolute size of droplet clusters, as given by the correlation length ξ, depends on the molar ratio of water to surfactant w.[5] This w dependency of ξ_0 is linear and was included in the fitting model as $\xi_0 = \xi_w \cdot w$ as discussed in Section 2.2.2. Fig. 10 therefore depicts the two w independent factors ξ_w and χ_0. Both pre-factors clearly decrease with increasing polymer content, while again the $Z = 1$ samples deviate from the overall trend. This is excluded from further analysis. The two dashed lines are fits of an exponential decay with an equal slope as the guide for the eye.

The susceptibility χ is in general proportional to an osmotic compressibility.[5] Thus the reduction of χ_0 under polymer addition can be interpreted as a decrease in the compressibility which in turn means a stiffening of the microemulsion droplets. Usually this stiffening is associated with an increase in percolation temperatures.[13,58] This observation is not fully supported by our dielectric measurements since a varying droplet size leads to different shifts of the percolation temperature under polymer addition (see Section 3.1).

The similar decrease of the pre-factor ξ_w can on one hand be interpreted as a reduction of the absolute cluster size close to the percolation with increasing polymer content. On the other hand, since $\xi_0 = \xi_w \cdot w$, the size of the single droplets has a smaller influence on the cluster size of polymer loaded microemulsions than on the polymer free ones. In contrast to the

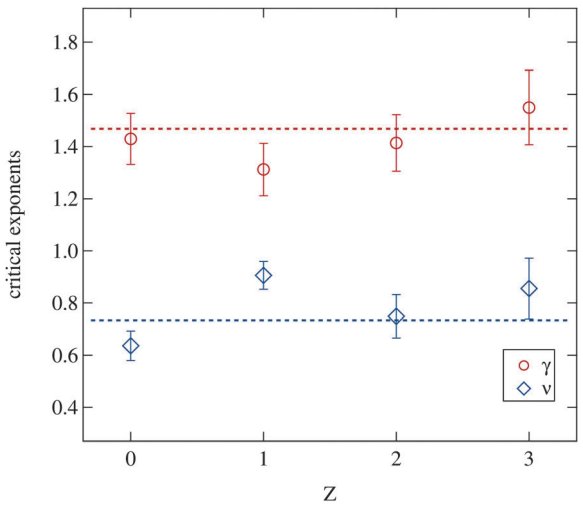

Fig. 9 Critical exponents γ and ν retrieved from the Ornstein–Zernike part of the structure factor (eqn (3) and (5)). Dashed lines are fitted constants to all data points with the premise $\gamma = 2\nu$.

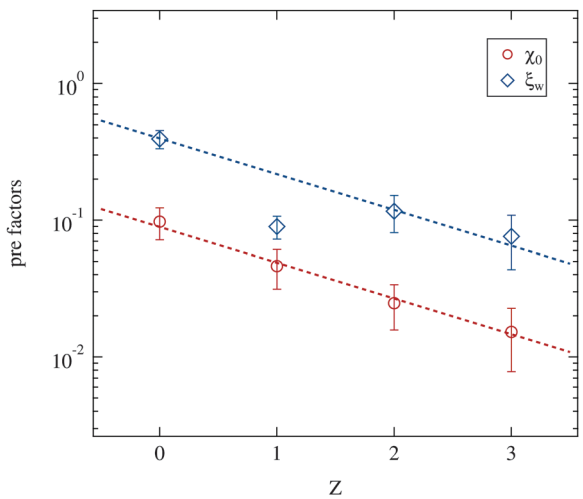

Fig. 10 Pre-factors ξ_w and χ_0 retrieved from the Ornstein–Zernike part of the structure factor (eqn (3) and (5)). Dashed lines are guides for the eye with an identical slope.

critical exponents γ and ν the pre-factors χ_0 and ξ_w show a clear dependency on the presence of the polymer. The phase transition itself taking place at the phase separation temperature T_c is thus not modified by the addition of PEG, while the detailed structural features as cluster sizes for example are determined by the polymer concentration per droplet.

3.3 Bending modulus of the surfactant layer

Using the results from the dynamic investigations by dielectric spectroscopy and the structural analysis by small angle X-ray scattering it is now possible to obtain the bending modulus of the surfactant shell of the microemulsion droplets. In detail we combine percolation temperatures and droplet radii. As predicted by eqn (8) the logarithm of the droplet radius at the percolation threshold should scale with the corresponding inverse percolation temperature. The slope of this linear dependency then is proportional to the bending modulus κ. Most publications making use of this relation directly measure the percolation temperature by dielectric spectroscopy but estimate the droplet radius by the simple equation $r_c \propto w$.[13,18] Others determine the droplet radius at room temperature by small angle X-ray scattering and assume the changes by heating up to the percolation temperature as negligible.[17] Both approaches are problematic as we have seen by analysing the form factor in Section 3.2.2. The droplet radius at T_p can deviate strongly from the simple estimation mentioned above or from its room temperature value.

In Fig. 11 the logarithmically scaled droplet radius r_c is plotted against the inverse percolation temperature T_p in order to check if eqn (8) holds true for the investigated systems even under polymer addition. The upper tile of the figure uses the droplet radii determined for each sample at 25 °C, while for the lower tile the radii were obtained at the individual percolation temperature of the sample. In both representations the linear dependency of the quantities predicted by eqn (8) can be seen, although the smallest droplets show some deviations for $Z = 0$ and $Z = 1$ if radii are determined at T_p. Addition of the polymer to the microemulsion droplets clearly does not affect the validity of the relation, but influences its slope and thus the bending modulus. The solid lines are fits of eqn (8) to the different Z series. While the data points in the upper tile of Fig. 11 are densely packed and do not seem to depend systematically on Z, the radii evaluated at T_p in the lower tile show an increasing slope with rising Z. Furthermore the different lines again intersect at one temperature which is around 1000 K/$T_p \approx 3.15$ thus $T_p \approx 45$ °C precisely the intersection temperature we already determined for $c(T)$ in Fig. 7. Such intersection points by the determination of the bending modulus under addition of polymers have been found before but at different temperatures which might be due to different molecular weights of the added polymer or the determination of the droplet radius at room temperature.[14,17]

Since for both methods of determining the droplet radius eqn (8) is fulfilled for all polymer concentrations it is possible to evaluate the Z dependent bending modulus κ. Fig. 12 presents the results of this evaluation and compares both approaches. The absolute value of $\kappa \approx k_B T$ for the polymer free systems is in good agreement with the literature.[13,14,17,18,21,59–61] For the polymer

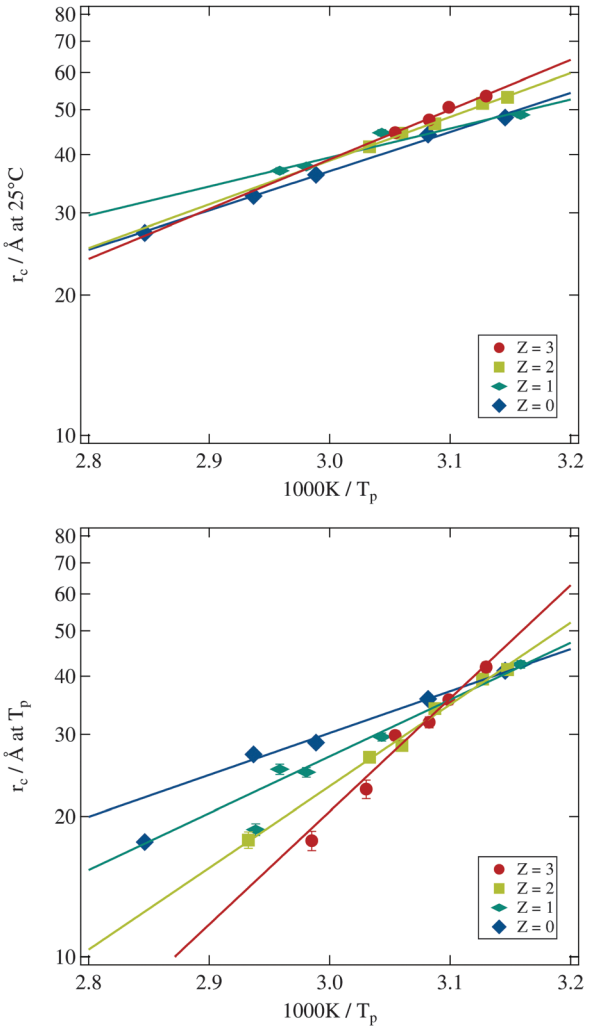

Fig. 11 Logarithmic droplet radius plotted against the inverse percolation temperature in kelvin. Upper tile: Droplet radii determined at $T = 25$ °C. Lower tile: Droplet radii determined at $T = T_p$. Error bars are smaller than symbols if not visible.

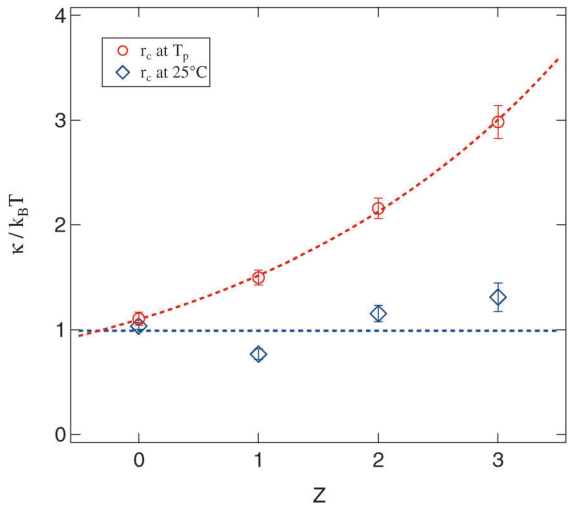

Fig. 12 Bending modulus of the surfactant shell evaluated by eqn (8) and its dependency on the number of polymer chains per droplet Z. Dashed lines are guides for the eye.

loaded systems a significant difference between the radius evaluation at 25 °C and at T_p exists. While for the former the bending modulus is rather constant under polymer addition the latter one shows a strongly increasing bending modulus up to a factor of three in comparison to the $Z = 0$ sample.

The basic assumption underlying eqn (8) is that at the percolation threshold T_p the persistence length ξ_K becomes equal to the droplet radius r_c.[18] Obviously this droplet radius has to be the one at the percolation temperature and not the one at room temperature or somewhere else. In conclusion the physically relevant curve in Fig. 12 is the upper one showing the strongly increasing bending modulus under polymer addition. This interpretation is further supported by the decreasing osmotic compressibility determined from the susceptibility χ of the Ornstein–Zernike structure factor part, which also points towards a stiffening of the surfactant shell (see Section 3.2.3).

4 Conclusions

Two transition phenomena are observed in the droplet phase of AOT based microemulsions: the dynamic percolation at $T = T_p$ and phase separation at the transition temperature $T = T_c$. These transitions are controlled by interdroplet interaction and the stability of the surfactant layer. When adding a polymer (PEG) to the water core of the droplets one finds a variation of the transition temperatures. Here we try to determine the bending modulus of the surfactant layer and its variation with the addition of the polymer. Experimentally we base our results on the determination of the droplet structure and on measurements with dielectric spectroscopy. Both transitions show up clearly in the variation of conductivity with temperature. We can thus study a wide range of droplet size, temperature and polymer content of the droplets.

Initially both temperatures, T_p and T_c, did not show a systematic dependency on the number of polymer chains per droplet. While for small droplets a decrease of the temperatures was observed the opposite holds true for larger droplets, an observation which has been reported in the literature.[14,17] In order to understand these observations experiments have to be extended to cover a maximum range of parameters and in particular the comparison of results from different experiments needs careful calibration of temperature.

For the structural investigations small angle X-ray scattering was used and we proposed a rather complex global fitting model, fixing several correlations between structure factor parameters in order to obtain reliable results. Here we make use of established dependencies of the structure on the composition of the system and temperature. This model provided a very good description of the experimental results. We were thus able to describe all data curves in the full recorded range of scattering vectors. The water core radius r_c and its polydispersity σ were found to obey the linear dependence on the molar ratio of water to surfactant w. This law prevailed even for systems with added polymer. The temperature dependent proportionality constant $c(T)$ decreased for all polymer contents with increasing T but changed from a linear to a quadratic decay for higher Z. For $T = 45$ °C the proportionality constant was found to be equal for all values of Z thus independent of the presence of polymers. Droplets are stable with respect to the addition of PEG.

Looking into the structure factor parameters the critical phenomena leading to the second order phase transition at T_c are not influenced by the presence of polymers. The critical exponents ν and γ of the correlation length ξ and the susceptibility χ obeyed the theoretically predicted scaling law $\gamma = 2\cdot\nu$ and are in good agreement with other investigations on microemulsion systems.[3,5,31,57] However, prefactors ξ_w and χ_0 revealed that the cluster formation in polymer loaded systems is less dependent on the single droplet radius and that compressibility is reduced upon polymer addition.

Finally by a combination of structural and dynamic results we showed that the evaluation of the bending modulus κ of the surfactant shell depends crucially on the correct determination of the droplet radii right at the percolation threshold. If this is correctly taken into account the bending modulus is found to increase significantly under polymer addition up to a factor of three for the largest investigated values of Z.

Acknowledgements

Financial support from the "Deutsche Forschungsgemeinschaft" DFG through the "DFG-Forschergruppe 1583", project STU191/6-1, is thankfully acknowledged.

References

1 C. Stubenrauch, *Microemulsions*, John Wiley & Sons, 2008.
2 S. H. Chen, *Annu. Rev. Phys. Chem.*, 1986, **37**, 351–399.
3 M. Kotlarchyk, S. H. Chen and J. S. Huang, *Phys. Rev. A: At., Mol., Opt. Phys.*, 1983, **28**, 508–511.
4 T. Spehr, B. Frick, I. Grillo and B. Stühn, *J. Phys.: Condens. Matter*, 2008, **20**, 104204.
5 M. Domschke, M. Kraska, R. Feile and B. Stühn, *Soft Matter*, 2013, **9**, 11503–11512.
6 M. Kraska, B. Kuttich and B. Stühn, in *Bottom-Up Self-Organization in Supramolecular Soft Matter*, ed. S. C. Müller and J. Parisi, Springer International Publishing, 2015, vol. 217, pp. 11–64.
7 A. Weber and B. Stühn, *J. Chem. Phys.*, 2016, **144**, 144903.
8 W. Helfrich, *Zeitschrift für Naturforschung. Teil C: Biochemie, Biophysik, Biologie, Virologie*, 1973, **28**, 693–703.
9 P. G. D. Gennes and C. Taupin, *J. Phys. Chem.*, 1982, **86**, 2294–2304.
10 L.-M. Wang, F. He and R. Richert, *Phys. Rev. Lett.*, 2004, **92**, 095701.
11 T. Blochowicz, E. Gouirand, A. Fricke, T. Spehr, B. Stühn and B. Frick, *Chem. Phys. Lett.*, 2009, **475**, 171–174.
12 S. Shipovskov, C. L. P. Oliveira, S. V. Hoffmann, L. Schauser, D. S. Sutherland, F. Besenbacher and J. S. Pedersen, *ChemPhysChem*, 2012, **13**, 3179–3184.

13 R. Wipf, S. Jaksch and B. Stühn, *Colloid Polym. Sci.*, 2010, **288**, 589–601.
14 M. Appel, T. Spehr, R. Wipf, C. Moers, H. Frey and B. Stühn, *J. Chem. Phys.*, 2013, **139**, 184903.
15 M. Laguës, *J. Phys., Lett.*, 1979, **40**, 331–333.
16 S. Geiger, H. F. Eicke and D. Spielmann, *Zeitschrift für Physik B Condensed Matter*, 1987, **68**, 175–179.
17 B. Kuttich, P. Falus, I. Grillo and B. Stühn, *J. Chem. Phys.*, 2014, **141**, 084903.
18 W. Meier, *Langmuir*, 1996, **12**, 1188–1192.
19 G. Gompper and D. M. Kroll, *Statistical Mechanics of Membranes and Surfaces*, World Scientific Publishing Co. Pte. Ltd., 2004, ch. Triangulatated-Surface Models of Flutctuating membranes, pp. 359–421.
20 B. Farago, D. Richter, J. S. Huang, S. A. Safran and S. T. Milner, *Phys. Rev. Lett.*, 1990, **65**, 3348–3351.
21 T. Spehr, B. Frick, I. Grillo, P. Falus, M. Müller and B. Stühn, *Phys. Rev. E: Stat., Nonlinear, Soft Matter Phys.*, 2009, **79**, 031404.
22 M. van Dijk, J. Joosten, Y. Levine and D. Bedeaux, *J. Phys. Chem.*, 1989, **93**, 2506–2512.
23 Q. Ying and B. Chu, *Macromolecules*, 1987, **20**, 362–366.
24 H. Wagner and R. Richert, *J. Phys. Chem. B*, 1999, **103**, 4071–4077.
25 G. R. Strobl, *Acta Crystallogr., Sect. A: Cryst. Phys., Diffr., Theor. Gen. Crystallogr.*, 1970, **26**, 367–375.
26 A. Guinier, *X-Ray Diffraction In Crystals, Imperfect Crystals and Amorphous Bodies*, Dover Publications, 1987.
27 N. W. Ashcroft and J. Lekner, *Phys. Rev.*, 1966, **145**, 83–90.
28 D. I. Svergun, P. V. Konarev, V. V. Volkov, M. H. J. Koch, W. F. C. Sager, J. Smeets and E. M. Blokhuis, *J. Chem. Phys.*, 2000, **113**, 1651–1665.
29 M. Müller, B. Stühn, K. Busse and J. Kressler, *J. Colloid Interface Sci.*, 2009, **335**, 228–233.
30 M. Kotlarchyk, S. H. Chen, J. S. Huang and M. W. Kim, *Phys. Rev. A: At., Mol., Opt. Phys.*, 1984, **29**, 2054–2069.
31 J. S. Huang and M. W. Kim, *Phys. Rev. Lett.*, 1981, **47**, 1462–1465.
32 T. Fließbach, *Statistische Physik*, Spketrum Akademischer Verlag GmbH, 1999.
33 H. F. Eicke, M. Borkovec and B. Das-Gupta, *J. Phys. Chem.*, 1989, **93**, 314–317.
34 N. Kallay and A. Chittofrati, *J. Phys. Chem.*, 1990, **94**, 4755–4756.
35 G. S. Grest, I. Webman, S. A. Safran and A. L. R. Bug, *Phys. Rev. A: At., Mol., Opt. Phys.*, 1986, **33**, 2842–2845.
36 M. Borkovec, H.-F. Eicke, H. Hammerich and B. D. Gupta, *J. Phys. Chem.*, 1988, **92**, 206–211.
37 D. Stauffer and A. Aharony, *Introduction To Percolation Theory*, Crc Pr Inc, 1994.
38 G. Gompper and D. M. Kroll, *J. Phys. I*, 1996, **6**, 1305–1320.
39 G. Ahlers, in *Pattern Formation in Liquid Crystals*, ed. A. Buka and L. Kramer, Springer New York, 1996, pp. 165–220.
40 G. W. Smith, G. M. Ventouris and J. L. West, *Mol. Cryst. Liq. Cryst. Sci. Technol., Sect. A*, 1992, **213**, 11–30.
41 D. Schübel, O. D. Bedford, G. Ilgenfritz, J. Eastoe and R. K. Heenan, *Phys. Chem. Chem. Phys.*, 1999, **1**, 2521–2525.
42 P. Ekwall, L. Mandell and K. Fontell, *J. Colloid Interface Sci.*, 1970, **33**, 215–235.
43 K. Fontell, *J. Colloid Interface Sci.*, 1973, **44**, 318–329.
44 H.-F. Eicke and J. Rehak, *Helv. Chim. Acta*, 1976, **59**, 2883–2891.
45 A. Maitra, *J. Phys. Chem.*, 1984, **88**, 5122–5125.
46 S.-H. Chen, S.-L. Chang and R. Strey, *J. Chem. Phys.*, 1990, **93**, 1907–1918.
47 Z. X. Li, J. R. Lu, R. K. Thomas and J. Penfold, *Trends in Colloid and Interface Science IX*, Steinkopff, 1995, vol. 98, pp. 243–247.
48 M. Kotlarchyk, S. H. Chen and J. S. Huang, *J. Phys. Chem.*, 1982, **86**, 3273–3276.
49 E. Y. Sheu, S.-H. Chen, J. S. Huang and J. C. Sung, *Phys. Rev. A: At., Mol., Opt. Phys.*, 1989, **39**, 5867–5876.
50 D. F. Evans and H. Wennerström, *The Colloidal Domain*, Wiley-VCH, 1999, ch. Micro- and Macroemulsions, pp. 548–561.
51 Y. Kawabata, H. Seto, M. Nagao and T. Takeda, *J. Chem. Phys.*, 2007, **127**, 044705.
52 K. Devanand and J. C. Selser, *Macromolecules*, 1991, **24**, 5943–5947.
53 S. Kawaguchi, G. Imai, J. Suzuki, A. Miyahara, T. Kitano and K. Ito, *Polymer*, 1997, **38**, 2885–2891.
54 A. Eliassi, H. Modarress and G. A. Mansoori, *J. Chem. Eng. Data*, 1998, **43**, 719–721.
55 P. G. D. Gennes, *J. Phys. Chem.*, 1990, **94**, 8407–8413.
56 B. Hammouda, D. Ho and S. Kline, *Macromolecules*, 2002, **35**, 8578–8585.
57 R. Aschauer and D. Beysens, *Phys. Rev. E: Stat. Phys., Plasmas, Fluids, Relat. Interdiscip. Top.*, 1993, **47**, 1850–1855.
58 S. K. Mehta and S. Sharma, *J. Colloid Interface Sci.*, 2006, **296**, 690–699.
59 J. S. Huang, S. T. Milner, B. Farago and D. Richter, *Phys. Rev. Lett.*, 1987, **59**, 2600–2603.
60 B. P. Binks, J. Meunier, O. Abillon and D. Langevin, *Langmuir*, 1989, **5**, 415–421.
61 E. van der Linden, S. Geiger and D. Bedeaux, *Phys. A*, 1989, **156**, 130–143.